Biogeosciences Discuss., 11, 7775–7796, 2014
www.biogeosciences-discuss.net/11/7775/2014/
doi:10.5194/bgd-11-7775-2014

Biogeosciences Discussions
Open Access

Global analysis of radiative forcing from fire-induced shortwave albedo change

G. López-Saldaña, I. Bistinas, and J. M. C. Pereira

Centro de Estudos Florestais, Instituto de Agronomia, Universidade de Lisboa, Tapada da Ajuda, 1349-017 Lisboa, Portugal

Received: 30 April 2014 – Accepted: 13 May 2014 – Published: 28 May 2014

Correspondence to: G. López-Saldaña (gerardolopez@isa.utl.pt)

Published by Copernicus Publications on behalf of the European Geosciences Union.

Abstract

Land surface albedo, a key parameter to derive Earth's surface energy balance, is used in the parameterization of numerical weather prediction, climate monitoring and climate change impact assessments. Changes in albedo due to fire have not been fully investigated at continental and global scale. The main goal of this study therefore, is to quantify the changes in albedo produced by biomass burning activities and their associated shortwave radiative forcing.

The study relies on the Moderate Resolution Imaging Spectroradiometer (MODIS) MCD64A1 burned area product to create an annual composite of areas affected by fire and the MCD43C2 BRDF-Albedo snow-free product to compute a bihemispherical reflectance time series. The approximate day of burn is used to calculate the instantaneous change in shortwave Albedo. Using the corresponding National Centers for Environmental Prediction (NCEP) monthly mean downward solar radiation flux at the surface, the global radiative forcing associated to fire was computed.

The analysis reveals a mean decrease in shortwave albedo of −0.023 ($1\sigma = 0.018$) causing a mean positive radiative forcing of 6.31 $W\,m^{-2}$ ($1\sigma = 5.04$) over the 2002–2012 time period in areas affected by fire. The greatest drop in mean shortwave albedo change occurs in 2002, which corresponds to the highest total area burnt (3.66 Mha) observed in the same year and produces the highest mean radiative forcing (6.75 $W\,m^{-2}$).

Africa is the main contributor in terms of burned area but forests globally are giving the highest radiative forcing per unit area, thus give detectable changes in shortwave albedo. The global mean radiative forcing for the whole studied period $\sim 0.04\,W\,m^{-2}$ shows that the contribution of fires into the Earth system is not insignificant.

BGD
11, 7775–7796, 2014

1 Introduction

Land-surface conditions have a strong impact on the Earth's system energy balance through changes in land surface albedo that induce a radiative forcing by perturbing the shortwave radiation budget (Ramaswamy et al., 2001). The total solar incoming radiation has a mean strength of $\sim 1366\,W\,m^{-2}$ ("solar constant") and has an irregular cycle of about 11 years, causing a variation of $\pm 0.5\,W\,m^{-2}$ (Gray, 2010). Since, on average, the Earth absorbs energy at the rate of $(1 - A)I_{TS}/4$ (Gray, 2010), where A is the Earth's albedo and I_{TS} the total solar irradiance, taking $I_{TS} = 1366\,W\,m^{-2}$ and a mean albedo of the Earth $A = 0.3$ (Prentice at al., 2012), the solar power available to the whole Earth system is $239.05\,W\,m^{-2}$. The importance of quantifying changes in albedo arises here. The radiative forcing caused by CO_2 is $1.56\,W\,m^{-2}$ (Forster et al., 2007) while that of changing the planetary albedo by as little as 0.01 can produce a change of the radiation balance of $2.39\,W\,m^{-2}$, revealing the role that even small changes in albedo can have a substantial impact in the Earth system.

Fire has a strong influence on climate due to the release of atmospheric aerosols and gases and can modify surface albedo by removal of vegetation and deposition of ash and charcoal (Bowman, 2009). Earlier studies aimed to quantify the impact of fires on the land surface albedo. Govaerts at al. (2002) analysed a Meteosat albedo time series for 1996 in Northern Hemisphere Africa and estimated that fires are responsible for a relative albedo decrease as large as 25 %, while Jin and Roy (2005) used MODIS data to estimate a mean 2003 shortwave albedo change of −0.024 over all the burned areas in the Australian tropical savana, which exerted a shortwave surface radiative forcing of $6.23\,W\,m^{-2}$. However, studies over longer time periods at global scale are needed to improve the understanding of the influence of fire in the Earth system as an agent of land surface alteration and its impact on the energy balance.

The main goal of this study is to quantify the albedo changes due to global vegetation fires and the corresponding shortwave radiative forcing at the surface. The radiative forcing contributed by aerosols produced by fires is not considered, since the scope of

BGD
11, 7775–7796, 2014

the study is to investigate exclusively the impact of fires at the surface. We derived an albedo time series and then calculated the difference in the pre- and post-fire shortwave albedo only in areas affected by fire for the 2002–2012 time period. The radiative forcing exerted by the changes in albedo was calculated using the total solar incoming radiation.

2 Data

2.1 Albedo time series generation and burned area identification

The shortwave albedo time series was generated using the MODerate-resolution Imaging Spectroradiometer (MODIS) Collection 5 BRDF/Albedo snow-free quality product (MCD43C2) (Schaaf et al., 2002). It is produced on a 16 day basis with an 8 day overlap projected to a 0.05° latitude/longitude Climate Modelling Grid (CMG). The product models the surface anisotropy using all high quality, cloud-free, snow-free and atmospherically corrected land surface reflectance obtained within a 16 day time period. When there are more than seven of these observations, a so-called *full model* inversion is attempted to retrieve the BRDF parameters based on the RossThickLiSparse-Reciprocal Bidirectional Distribution Reflectance (BRDF) model (Lucht et al., 2000). If there are only 3 to 6 of the aforementioned observations over the 16-dat time period, a backup algorithm is used, it is based on a archetypal BRDF model parameters which is defined with respect to 25 global land cover classes and from historical high quality retrievals (Ju et al., 2010). Data for 11 years, 2002 to 2012 was downloaded from the Land Processes Distributes Active Archive Center (LP DAAC) data pool.

In order to use only the highest quality data, the BRDF_Quality science data set provided with the MCD43C2 was analysed. Only pixels with *best quality* (75 % or more with best full inversions) and *good quality* (75 % or more with full inversions) were kept for further processing. Using the three BRDF model parameters, the isotropic f_{iso}, volumetric f_{vol} and geometric f_{geo}, from the shortwave broadband (0.3–5.0 µm) the

BGD
11, 7775–7796, 2014

global bihemispherical reflectance (BHR) under isotropic illumination named as well as white-sky albedo for every 16 day time period was computed using:

$$\alpha_{\mathrm{BHR}}(\lambda) = f_{\mathrm{iso}}(\lambda)g_{\mathrm{iso}} + f_{\mathrm{vol}}(\lambda)g_{\mathrm{vol}} + f_{\mathrm{geo}}(\lambda)g_{\mathrm{geo}} \quad (1)$$

and the integrated coefficients shown in Table 1.

Some areas can show gaps caused by lack of high quality data and by the screening based on the BRDF_Quality flag. A linear temporal interpolation was computed to create a synthetic, temporally and spatially continuous shortwave albedo product. The interpolation was performed on a yearly basis but taking into account one month before and after the calendar year to be able to fill gaps at the very beginning or at the very end of the year. The final product consists of a gap-free 16 day (with an 8 day overlap) snow-free broadband shortwave albedo time series with a 0.05° spatial resolution for 2002 to 2012.

2.2 Burned area identification

The areas affected by fire per year were derived using the MODIS Collection 5.1 Direct Broadcast Monthly Burned Area Product (MCD64A1) (Gilgio et al., 2009). The product identifies post-fire burned areas using daily 500 m surface reflectance coupled with 1 km MODIS active fires observations. Twelve years of data were downloaded from (MCD64A1 burned area product) spanning from 2002 to 2012. The spatial resolution of the product is 500 m and is generated on a monthly basis. It was necessary to perform a spatial aggregation on the monthly datasets to 0.05° using a mode filter to match the CMG spatial resolution. The annual burned area dataset was generated selecting the approximate day of burned from the monthly datasets. When more than one day was found the earliest date was selected.

BGD
11, 7775–7796, 2014

2.3 Land Use Land Cover (LULC) maps

The MODIS Collection 5.1 Land Cover Type Yearly (MCD12C1) (Friedl et al., 2010) is produced at 0.05° spatial resolution and provides the dominant land cover type and the sub-grid frequency land cover class distribution within each 0.05° cell.

In order to analyse major biomes an aggregation of the land cover classes was performed. For every year from 2002 to 2012: (1) all forest classes (evergreen needleleaf forest, evergreen broadleaf forest, deciduous needleleaf forest, deciduous broadleaf forest, mixed forests) were aggregated into a single "Forest" class, (2) croplands, cropland/natural vegetation mosaic was aggregated into the "Croplands" class and (3) closed shrubland, open shrublands, woody savannas, savannas, grasslands and permanent wetlands were aggregated into the "non-forest" class. The aggregation takes into account the confidence level, only when confidence was bellow 60 % the "majority land cover type 2" was used.

Additionally to the analysis per land cover, an analysis per continent will be performed. The regions used in the study are depicted in Fig. 1.

2.4 Downward shortwave solar radiation flux at the surface

The National Centers for Environmental Prediction and the National Center for Atmospheric Research (NCEP/NCAR) Reanalysis 1 (Kalnay et al., 1996) provides the monthly mean downward solar radiation flux (dswrf) at the surface in $W\,m^{-2}$ at 1.8° by 1.8° grid cells from 1948 to 2013. The full reanalysis dataset was obtained from (NCEP/NCAR dswrf at the surface). A temporal subset was extracted to obtain 12 years of monthly dswrf from 2002 to 2012.

BGD
11, 7775–7796, 2014

3 Quantification of albedo change and associated radiative forcing

3.1 Method description

For every pixel identify as affected by fire within a calendar year, the change in broadband shortwave albedo is calculated as

$$\Delta A_{\text{fire}} = A_{\text{post}} - A_{\text{pre}} \quad (2)$$

where ΔA_{fire} is the "instantaneous" land surface shortwave albedo change when subtracting the pre-fire albedo (A_{pre}) from the post-fire albedo (A_{post}).

The selection of the dates to compute the change in albedo is not straightforward, and several factors must be taken into account.

First, the albedo time series was computed using the BRDF model parameters and these parameters were derived fitting a BRDF model using all high quality observations within a 16 day time period. The assumption is that even when there may be day-to-day changes in land surface condition these high quality observations have normally distributed random noise and can describe the BRDF (Lucht and Lewis, 2000). However, fire affects vegetated areas, which generally are very reflective in the near-infra-red and after a burning event show a decrease in reflectance due to vegetation loss and deposition of charcoal and ash (Pereira, 1999; Stroppiana, 2002). Additionally some fire events may last more than one day in several areas around the globe (Chuvieco et al., 2008). Therefore the 16 day time periods adjacent to the approximate day of burned might have used mixed observations, burned and non-burned, to fit the BRDF model resulting in a smooth transition from the pre-fire to post-fire albedo rather than a sharp change.

Second, there is uncertainty in the day of burning. The MCD64A1 product relies on both, daily surface reflectance and daily fire masks. However, a minimum of approximately ten days of cloud-free observations before and after to accommodate the moving windows employed in the change-detection process are needed, lack of data due to clouds or coverage gaps double the number of days required (Gilgio et al.,

BGD
11, 7775–7796, 2014

2009). Additionally the Quality Assessment (QA) Scientific Dataset (SDS) masks surface reflectance pixels when an active fire is detected, which increases the temporal uncertainty in the identification of the day of burned.

Given these two factors, an analysis to quantify the length of the window, centred at the approximate day of burn, which is needed to compute the change in albedo was carried out. The result is that a 32 day window is the best to be used at global scale. The A_{pre} date was set identifying the maximum albedo previous to the fire occurrence, while the A_{post} date the minimum albedo value after the fire.

Ramaswamy et al. (2001) define the radiative forcing as 'the change in net (down minus up) irradiance (solar plus longwave; in W m^{-2}), and since for this study we neglect any longwave forcing, once the change in albedo ΔA_{fire} was computed, the shortwave radiative forcing at the surface $\Delta F_{surface}$ exerted by changes in shortwave albedo only due to fire is estimated as:

$$\Delta F_0 = -\text{dswrf}_0^{\downarrow} \Delta A_{fire}$$

where $-\text{dswrf}_0^{\downarrow}$ is the monthly mean downward solar radiation flux (dswrf) at the surface in W m^{-2}, the subscript ($_0$) denotes the quantity at the surface.

4 Results

Overall, the trend in mean annual radiative forcing for the whole studied period is negative, in agreement with the trend of the total annual area burnt (Fig. 2). The mean albedo changes, considering the change between post-fire shortwave albedo minus the pre-fire value, have the opposite trend of the total annual area burnt. Fundamentally, a fire event will decrease the shortwave albedo, resulting a positive radiative forcing in return (Figs. 5 and 6). The main discrepancies between area burnt and radiative forcing occur in the period of 2005–2007, where intermediate-high area burnt is associated with the lowest values of radiative forcing in 2005 and 2007, and a high abrupt peak in 2006.

BGD
11, 7775–7796, 2014

The greatest drop in mean shortwave albedo change occurs in 2002, which corresponds to the highest total area burnt (3.66 Mha) observed in the same year and produces the highest mean radiative forcing (6.75 $W m^{-2}$) (Fig. 2). The lowest shortwave albedo change values in 2005 and 2007 are not associated to low area burnt and similarly the lowest and very abrupt drop of area burnt in 2009 does not produce the lowest albedo change and radiative forcing (Fig. 2).

Most fires occur in the Sahel (Fig. 5) and the Australian savanas (Fig. 6) corresponding to an average up to 89 % of the total global area burnt, whereas the highest radiative forcing per unit area is located in forests of Europe in 2010, Australia in 2003 and 2006 and Asia in 2003, with mean continental values of 27 $W m^{-2}$, 20.4 and 21 $W m^{-2}$, and 15.3 $W m^{-2}$ respectively (Fig. 3). In croplands, Asia shows the highest radiative forcing and the greatest oscillations with a minimum of 6.79 $W m^{-2}$ in 2005 and maximum of 10.8 $W m^{-2}$ in 2003 (Fig. 3). The rest of the continents show a low variability in cropland areas, with the exception of Australia in 2003 showing a steep peak of 10.5 $W m^{-2}$. In non-forests, the highest radiative forcing is in North America in 2004, in Europe in 2010 and in Asia in 2003 and 2010. High oscillations are also observed in Australia with an abrupt drop in 2010, contrasting with very stable inter-annual cycle of Africa.

At the global scale, the highest mean radiative forcing occurs in forested areas, in 2003, in 2006 and in 2010. Croplands and non-forests have a stable inter-annual cycle with the exception of 2003 and 2004 respectively being the years with the highest mean values (Fig. 4).

The global mean change in albedo is -0.023 ($\sigma = 0.018$) causing a mean positive radiative forcing of 6.31 $W m^{-2}$ ($\sigma = 5.04$) on a global mean annual burned area of 349.48 Mha ($\sigma = 21.81$ Mha) during the 2002 to 2012 time period.

In order to quantify the global or regional impact, it is necessary to normalize the forcing by the proportion of the total area burned to the total surface. Given $r = 6\,371\,007.181$ m as the radius of the idealized sphere representing the Earth; the total global surface is $4\pi r^2$, ~ 510.07 Mkm^2. The mean annual global area affected by fires during the 11 years comprising the study period is 349.48 Mha or 3.4948 Mkm^2,

BGD
11, 7775–7796, 2014

$\sim 0.69\,\%$ of the Earth's surface. Since the mean radiative forcing only in areas where fire occurred during 2002–2012 is $6.31\,W\,m^{-2}$, the global mean radiative forcing is $\sim 0.04\,W\,m^{-2}$. When performing the same calculation at regional scale, for instance, Australia, the mean radiative forcing is $\sim 7.66\,W\,m^{-2}$, and the mean area burned is $0.502\,Mkm^2$, representing the $\sim 6.53\,\%$ of the Australian territory leading to a mean radiative forcing for Australia of $\sim 0.49\,W\,m^{-2}$, an order of magnitude higher than the global number.

5 Discussion and conclusions

We have presented a study to quantify the temporal evolution of fire-induced albedo changes and the continental and global annual mean forcing estimations. In here, we used the radiative forcing as a measure to quantify the influence and contribution of fire in the Earth's energy balance, and showed that fired caused a consistent decrease the land surface shortwave albedo, leading to a positive radiative forcing.

Continental Europe includes Russian territories and, has as eastern borders the Ural mountains, the Ural river and the Caucasus mountains, as well as the water line of Caspian lake. Therefore, the anomalous fire events in July 2010 around Moscow are included in European continent. On an annual basis, in Russia, 90–95 % of burnt areas are located in the Asian part of Russia with the majority (59.3 %) being forests, with the exception of the extreme event of 2010 (Shvidenko et al., 2011). The abrupt peak in 2010 in Fig. 3e corresponds to that event exactly with mean annual value for forests in continental Europe of $27\,W\,m^{-2}$. The mean continental value is more realistic when compared to the massive maximum number of $167\,W\,m^{-2}$ for the same event including aerosols in smoky conditions found in the literature (Chubarova et al., 2012).

Similar extreme events can be observed in Fig. 3f in 2003 and 2006 in Australia, depicting the Eastern Victorian alpine fires, which burnt 1.3 Mha in 2003, and the Grampians in Victoria in 2006 that burned 184 000 ha. A plausible explanation is that a weak to moderate El Niño event had a very strong impact in Australia causing the

BGD
11, 7775–7796, 2014

major 2002–2003 drought had rainfall deficiencies over the period March 2002 to January 2003 (Australian Government, 2014). Fires affected eastern New South Wales (NSW), Canberra, and the mountains areas of southeast NSW and forested areas in eastern Victoria as show in Fig. 6 upper-left panel. A radiative forcing above 15 W m^{-2} over northeast Victoria and the Great Dividing Range Mountains in the Kosciuszko National Park in southern NSW mainly to a large shortwave albedo decrease due to forest fires is shown in Fig. 6. Broadly, forest has a low shortwave albedo ~ 0.3 that varies with the viewing and illumination conditions (Liang, 2000). Given the extraordinary circumstances during the 2002–2003 drought in Australia, the forest fires dramatically altered the albedo, up to a 60 % relative change in some areas, during the Austral summer (pick of incoming radiation), nevertheless changes due to seasonality, e.g., vegetation senescence that affects surface reflectivity were not taking into account and a contribution of the decrease in albedo in the Australian summer might be due to these non-fire related changes.

In Fig. 3b, the highest value of radiative forcing occurs in 2003 when the massive boreal fires in western Siberia burning over 20 Mha and being one of the largest forest fires on record (Sheng et al., 2004). Croplands and non-forests are following the west Siberian event of 2003, showing the highest mean radiative forcing value of all cropland areas (Fig. 3b).

In North America in 2004 there is the highest continental value of mean annual radiative forcing occurring in non-forests (15.38 W m^{-2}). The summer of 2004 was an extensive fire season in Alaska and western Canada with the majority of the area burnt happening grasslands (including shrublands) and forests (Turquety et al., 2007).

In South America the three-year intervals of increased radiative forcing might be associated to teleconnections causing extensive droughts like in 2010 (Lewis et al., 2011), that increase fire incidence in forests and savanas, but also to anthropogenic activities (Aragão and Shimabukuro, 2010).

A global mean radiative forcing estimation of ~ 0.04 W m^{-2} quantifies the contribution of fire to the Earth's system, in which forest fires show the most dramatic impact per

BGD
11, 7775–7796, 2014

area unit. Large extreme events can be detected in annual basis and show abrupt changes in shortwave albedo and its associated radiative forcing. Although the fire incidence in Africa is the highest with little inter-annual oscillations, the biggest changes in annual radiative forcing is caused by the extreme fire events in Australia, Europe and North America.

Anomalous fire events in continental Australia along with the boreal forests drive the global annual extremes of mean radiative forcing and show an excellent opportunity for future research efforts in that field.

Acknowledgements. The research leading to these results has received funding from the European Community's Seventh Framework Programme (FP7 2007-2013) under grant agreement n° 238366. For all our colleagues at LDRAG, thank you for your support. Duarte Oom: SMA&D&N.

References

Aragão, L. E. O. C. and Shimabukuro, Y. E.: The incidence of fire in Amazonian forests with implications for REDD, Science, 328, 1275–1278, doi:10.1126/science.1186925, 2010.

Australian Government: available at: http://www.bom.gov.au/climate/enso/enlist/ (last access: 30 April 2014), 2014.

Boisier, J. P., de Noblet-Ducoudré, N., and Ciais, P.: Inferring past land use-induced changes in surface albedo from satellite observations: a useful tool to evaluate model simulations, Biogeosciences, 10, 1501–1516, doi:10.5194/bg-10-1501-2013, 2013.

Bowman, D. M. J. S., Balch, J. K., Artaxo, P., Bond, W. J., Carlson, J. M., Cochrane, M. A., D'Antonio, C. M., Defries, R. S., Doyle, J. C., Harrison, S. P., Johnston, F. H., Keeley, J. E., Krawchuk, M. A., Kull, C. A., Marston, J. B., Moritz, M. A., Prentice, I. C., Roos, C. I., Scott, A. C., Swetnam, T. W., van der Werf, G. R. and Pyne, S. J.: Fire in the Earth system, Science, 324, 481–484, doi:10.1126/science.1163886, 2009.

Chubarova, N., Nezval', Ye., Sviridenkov, I., Smirnov, A., and Slutsker, I.: Smoke aerosol and its radiative effects during extreme fire event over Central Russia in summer 2010, Atmos. Meas. Tech., 5, 557–568, doi:10.5194/amt-5-557-2012, 2012.

BGD
11, 7775–7796, 2014

Chuvieco, E., Giglio, L., and Justice, C.: Global characterization of fire activity: toward defining fire regimes from Earth observation data, Glob. Change Biol., 14, 1488–1502, doi:10.1111/j.1365-2486.2008.01585.x, 2008.

Friedl, M. A., Sulla-Menashe, D., Tan, B., Schneider, A., Ramankutty, N., Sibley, A., and Huang, X.: MODIS Collection 5 global land cover: algorithm refinements and characterization of new datasets, Remote Sens. Environ., 114, 168–182, doi:10.1016/j.rse.2009.08.016, 2010.

Forster, P., Ramaswamy, V., Artaxo, P., Berntsen, T., Betts, R., Fahey, D. W., Haywood, J., Lean, J., Lowe, D. C., Myhre, G., Nganga, J., Prinn, R., Raga, G., Schulz, M., and Van Dorland, R.: 2007: Changes in Atmospheric Constituents and in Radiative Forcing, in: Climate Change 2007: The Physical Science Basis. Contribution of Working Group I to the Fourth Assessment Report of the Intergovernmental Panel on Climate Change, edited by: Solomon, S., Qin, D., Manning, M., Chen, Z., Marquis, M., Averyt, K. B., Tignor, M., and Miller, H. L., Cambridge University Press, Cambridge, United Kingdom and New York, NY, USA, 129–234, 2007.

Giglio, L., Loboda, T., Roy, D. P., Quayle, B., and Justice, C. O.: An active-fire based burned area mapping algorithm for the MODIS sensor, Remote Sens. Environ., 113, 408–420, doi:10.1016/j.rse.2008.10.006, 2009.

Govaerts, Y. M., Pereira, J. M., Pinty, B., and Mota, B.: Impact of fires on surface albedo dynamics over the African continent, J. Geophys. Res., 107, 4629, doi:10.1029/2002JD002388, 2002.

Jin, Y. and Roy, D. P.: Fire-induced albedo change and its radiative forcing at the surface in northern Australia, Geophys. Res. Lett., 32, L13401, doi:10.1029/2005GL022822, 2005.

Gray, L. J., Beer, J., Geller, M., Haigh, J. D., Lockwood, M., Matthes, K., Cubasch, U., Fleitmann, D., Harrison, G., Hood, L., Luterbacher, J., Meehl, G. A., Shindell, D., van Geel, B., and White, W.: Solar Influences on Climate, Rev. Geophys., 48, RG4001, doi:10.1029/2009RG000282, 2010.

Ju, J., Roy, D. P., Shuai, Y., and Schaaf, C.: Development of an approach for generation of temporally complete daily nadir MODIS reflectance time series, Remote Sens. Environ., 114, 1–20, doi:10.1016/j.rse.2009.05.022, 2010.

Kalnay, E., Kanamitsu, M., Kistler, R., Collins, W., Deaven, D., Gandin, L., Iredell, M., Saha, S., White, G., Woollen, J., Zhu, Y., Leetmaa, A., Reynolds, R., Chelliah, M., Ebisuzaki, W., Higgins, W., Janowiak, J., Mo, K. C., Ropelewski, C., Wang, J., Jenne, R., and Joseph, D.: The NCEP/NCAR 40-Year Reanalysis Project, B. Am. Meteorol. Soc., 77, 437–471, 1996.

BGD
11, 7775–7796, 2014

Lewis, S. L., Brando, P. M., Phillips, O. L., van der Heijden, G. M. F., and Nepstad, D.: The 2010 Amazon drought, Science, 331, 554, doi:10.1126/science.1200807, 2011.
Liang, S.: Narrowband to broadband conversions of land surface albedo I algorithms, Remote Sens. Environ., 76, 213–238, 2001.
Lucht, W. and Lewis, P.: Theoretical noise sensitivity of BRDF and albedo retrieval from the EOS-MODIS and MISR sensors with respect to angular sampling, Int. J. Remote Sens., 21, 81–98, doi:10.1080/014311600211000, 2000.
Lucht, W., Schaaf, C. B., and Strahler, A. H.: An algorithm for the retrieval of albedo from space using semiempirical BRDF models, IEEE T. Geosci. Remote, 38, 977–998, doi:10.1109/36.841980, 2000.
MCD64A1 burned area product, available at: ftp://fuoco.geog.umd.edu/db/MCD64A1/ (last access: 24 April 2014), 2014.
NCEP/NCAR dswrf at the surface: available at: ftp://ftp.cdc.noaa.gov/Datasets/ncep.reanalysis.derived/surface_gauss/dswrf.sfc.mon.mean.nc (last access: 24 April 2014), 2014.
Pereira, J. M.: A comparative evaluation of NOAA/AVHRR vegetation indexes for burned surface detection and mapping, IEEE T. Geosci. Remote, 37, 217–226, doi:10.1109/36.739156, 1999.
Prentice, I. C., Baines, P. G., Scholze, M., and Wooster, M. J.: Fundamentals of climate change science, in: Understanding the Earth System: Global Change Science for Application, edited by: Cornell, S. E., Prentice, I. C., House, J. I., and Downy, C. J., Cambridge University Press, 39–71, 2012..
Ramaswamy, V., Boucher, O., Haigh, J. D., Hauglustaine, D., Haywood, J., Myhre, G., Nakajima, T., Shi, G. Y., and Solomon, S.: Radiative Forcing of Climate Change, in: Climate Change 2001: The Scientific Basis. Contribution of Working Group I to the Third Assessment Report of the Intergovernmental Panel on Climate Change, edited by: Houghton, J. T., Ding, Y., Griggs, D. J., Noguer, M., van der Linden, P. J., Dai, X., Maskell, K., and Johnson, C. A., Cambridge University Press, Cambridge, UK and New York, NY, USA, 349-416, 2001.
Schaaf, C. B., Gao, F., Strahler, A. H., Lucht, W., Li, X., Tsang, T., Strugnell, N. C., Zhange, X., Jin, Y., Muller, J. P., Lewis, P., Barnsley, M., Hobson, P., Disney, M., Roberts, G., Dunderdale, M., Doll, C., d'Entremont, R. P., Hu, B., Liang, S., Privett, J. L., and Roy, D.: First operational BRDF, albedo nadir reflectance products from MODIS, Remote Sens. Environ., 83, 135–148, 2002.

BGD
11, 7775–7796, 2014

Sheng, Y., Smith, L. C., MacDonald, G. M., Kremenetski, K. V., Frey, K. E., Velichko, A. A., Lee, M., Beilman, D. W., and Dubinin, P.: A high-resolution GIS-based inventory of the west Siberian peat carbon pool, Global Biogeochem. Cy., 18, GB3004, doi:10.1029/2003GB002190, 2004.

Shvidenko, A. Z., Shchepashchenko, D. G., Vaganov, E. A., Sukhinin, A. I., Maksyutov, S. S., McCallum, I., and Lakyda, I. P.: Impact of wildfire in Russia between 1998–2010 on ecosystems and the global carbon budget, Dokl. Earth Sci., 441, 1678–1682, doi:10.1134/S1028334X11120075, 2011.

Stroppiana, D., Pinnock, S., Pereira, J. M., and Grégoire, J.-M.: Radiometric analysis of SPOT-VEGETATION images for burnt area detection in Northern Australia, Remote Sens. Environ., 82, 21–37, doi:10.1016/S0034-4257(02)00021-4, 2002.

Turquety, S., Logan, J. A., Jacob, D. J., Hudman, R. C., Leung, F. Y., Heald, C. L., Yantosca, R. M., Wu, S., Emmons, L. K., Edwards, D. P., and Sachse, G. W.: Inventory of boreal fire emissions for North America in 2004: importance of peat burning and pyroconvective injection, J. Geophys. Res., 112, D12S03, doi:10.1029/2006JD007281, 2007.

van der Werf, G. R., Randerson, J. T., Giglio, L., Collatz, G. J., Mu, M., Kasibhatla, P. S., Morton, D. C., DeFries, R. S., Jin, Y., and van Leeuwen, T. T.: Global fire emissions and the contribution of deforestation, savanna, forest, agricultural, and peat fires (1997–2009), Atmos. Chem. Phys., 10, 11707–11735, doi:10.5194/acp-10-11707-2010, 2010.

BGD
11, 7775–7796, 2014

Table 1. Coefficients used for Eq. (1).

Terms g for kernel k	k = isotropic	k = RossThick (vol)	k = LiSparse-R (geo)
BHR (White-sky)	1.0	0.189184	−1.377622

BGD
11, 7775–7796, 2014

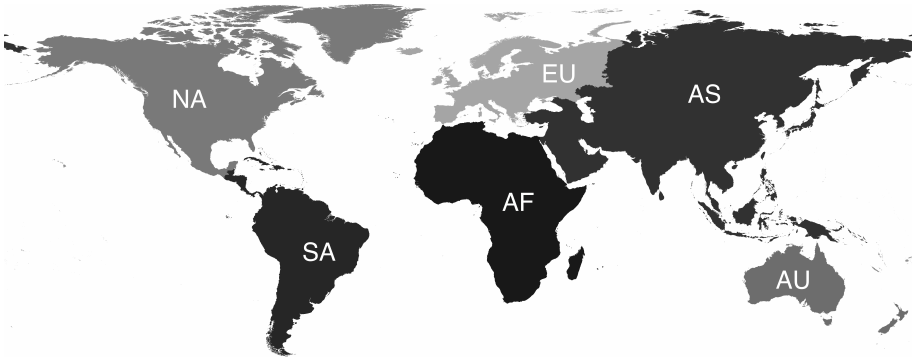

Figure 1. Regions used in analysis. North America (NA), South America (SA), Africa (AF), Europe (EU), Asia (AS) and Australia (AU).

BGD
11, 7775–7796, 2014

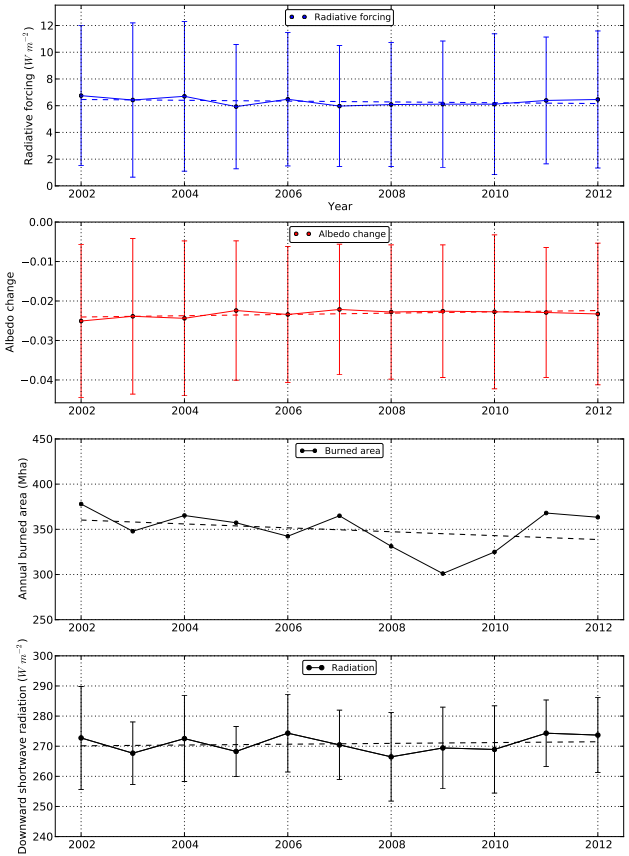

Figure 2. Temporal changes of the annual global radiative forcing induce by fires (blue line) and albedo change (in red) spanning from 2002 to 2012. Bottom plots show the total annual burned area and the downward shortwave radiation fluxes at the surface. The spatial variations (one standard deviation) in radiative forcing, albedo change and shortwave radiation are plotted as vertical bars. The dashed lines depict linear trends.

BGD
11, 7775–7796, 2014

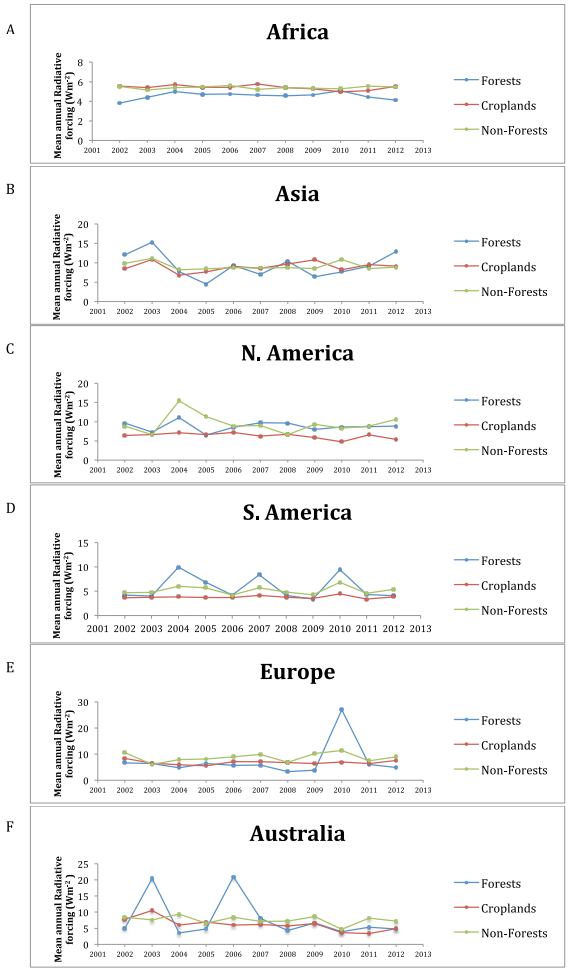

Figure 3. The mean annual radiative forcing per land cover and continent **(A–F)**.

BGD
11, 7775–7796, 2014

Global analysis of radiative forcing from fire-induced shortwave albedo change

G. López-Saldaña et al.

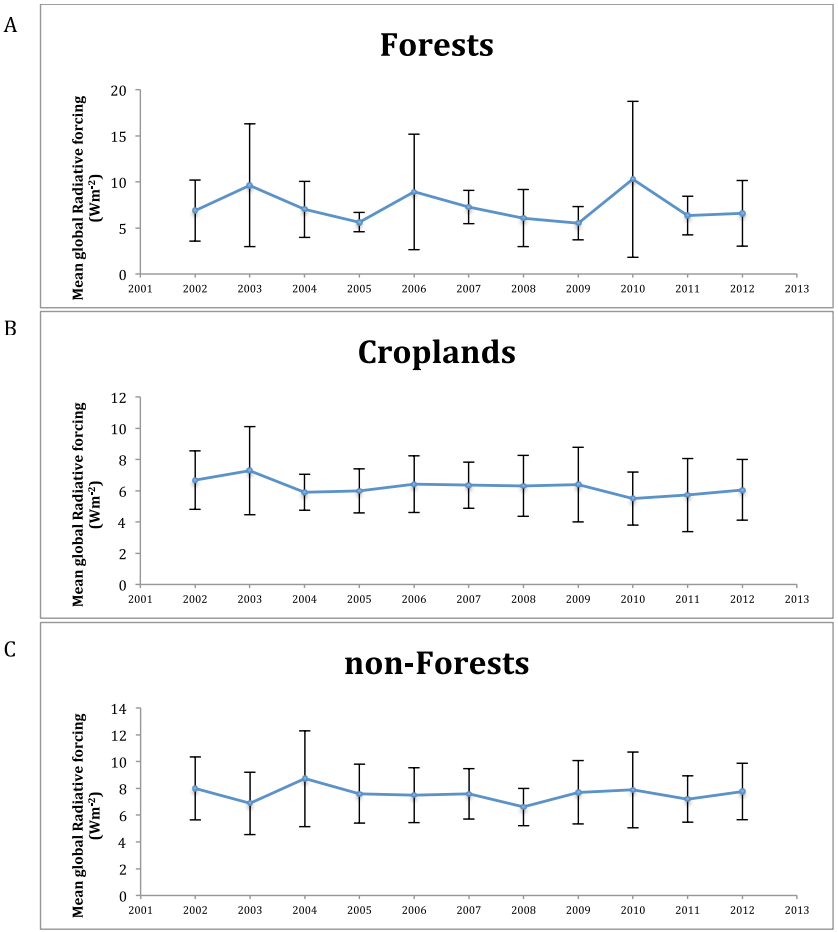

Figure 4. The mean annual radiative forcing per land cover **(A–C)** in W m^{-2}.

BGD
11, 7775–7796, 2014

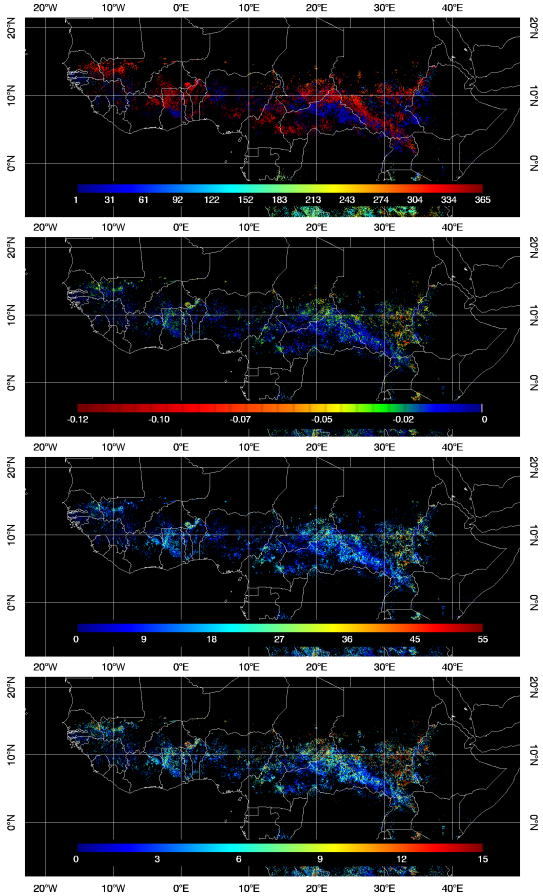

Figure 5. The approximate day of burn (top); the "instantaneous" shortwave albedo change in areas affected by fire (middle top); the relative change in albedo in % (mid bottom) and the associated radiative forcing in W m^{-2} (bottom) is shown for the Sahel during 2003.

BGD
11, 7775–7796, 2014

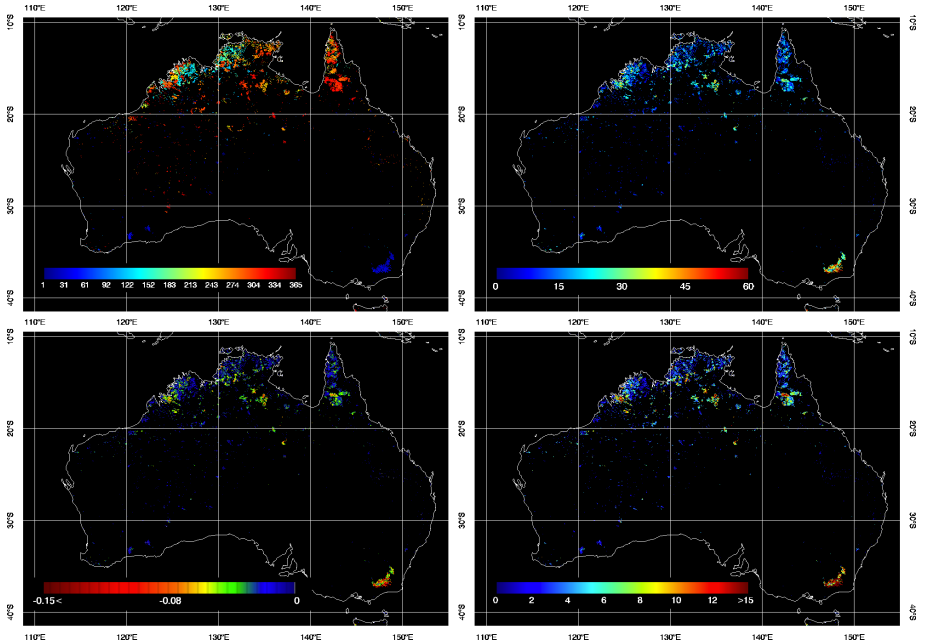

Figure 6. The approximate day of burn (top left); the "instantaneous" shortwave albedo change in areas affected by fire (bottom left); the relative albedo change in % (top right) and the associated radiative forcing in W m^{-2} (bottom right) is shown for Australia during 2003.

BGD
11, 7775–7796, 2014